be performed. Starting from the results presented here on the fungal FAS and on the architecturally distinct mammalian FAS described in an accompanying paper (*38*), it may even be possible to ultimately obtain a detailed atomic model for both types of FAS assemblies.

References and Notes

1. F. Lynen, *Eur. J. Biochem.* **112**, 431 (1980).
2. S. J. Wakil, J. K. Stoops, V. C. Joshi, *Annu. Rev. Biochem.* **52**, 537 (1983).
3. E. Schweizer, J. Hofmann, *Microbiol. Mol. Biol. Rev.* **68**, 501 (2004).
4. S. Smith, A. Witkowski, A. K. Joshi, *Prog. Lipid Res.* **42**, 289 (2003).
5. S. W. White, J. Zheng, Y. M. Zhang, C. O. Rock, *Annu. Rev. Biochem.* **74**, 791 (2005).
6. F. Fichtlscherer, C. Wellein, M. Mittag, E. Schweizer, *Eur. J. Biochem.* **267**, 2666 (2000).
7. F. Wieland, E. A. Siess, L. Renner, C. Verfürth, F. Lynen, *Proc. Natl. Acad. Sci. U.S.A.* **75**, 5792 (1978).
8. J. K. Stoops *et al.*, *J. Biol. Chem.* **253**, 4464 (1978).
9. W. A. Hackenjos, H. J. Schramm, *Biol. Chem. Hoppe Seyler* **368**, 19 (1987).
10. J. K. Stoops, S. J. Kolodziej, J. P. Schroeter, J. P. Bretaudiere, S. J. Wakil, *Proc. Natl. Acad. Sci. U.S.A.* **89**, 6585 (1992).
11. S. J. Kolodziej, P. A. Penczek, J. P. Schroeter, J. K. Stoops, *J. Biol. Chem.* **271**, 28422 (1996).
12. S. J. Kolodziej, P. A. Penczek, J. K. Stoops, *J. Struct. Biol.* **120**, 158 (1997).
13. D. W. Brown, T. H. Adams, N. P. Keller, *Proc. Natl. Acad. Sci. U.S.A.* **93**, 14873 (1996).
14. C. M. Watanabe, C. A. Townsend, *Chem. Biol.* **9**, 981 (2002).
15. C. P. Woloshuk, R. Prieto, *FEMS Microbiol. Lett.* **160**, 169 (1998).
16. K. Takayama, C. Wang, G. S. Besra, *Clin. Microbiol. Rev.* **18**, 81 (2005).
17. L. G. Dover, A. M. Cerdeño-Tárrága, M. J. Pallen, J. Parkhill, G. S. Besra, *FEMS Microbiol. Rev.* **28**, 225 (2004).
18. Materials and methods are described in the supporting material on *Science* Online.
19. J. G. Olsen *et al.*, *FEBS Lett.* **460**, 46 (1999).
20. M. Fisher *et al.*, *Struct. Fold. Design* **8**, 339 (2000).
21. K. M. Koski, A. M. Haapalainen, J. K. Hiltunen, T. Glumoff, *J. Mol. Biol.* **345**, 1157 (2005).
22. M. S. Kimber *et al.*, *J. Biol. Chem.* **279**, 52593 (2004).
23. D. Kostrewa, F. K. Winkler, G. Folkers, L. Scapozza, R. Perozzo, *Protein Sci.* **14**, 1570 (2005).
24. J. L. Fox, F. Lynen, *Eur. J. Biochem.* **109**, 417 (1980).
25. N. Nagano, C. A. Orengo, J. M. Thornton, *J. Mol. Biol.* **321**, 741 (2002).
26. Y. Lindqvist, C. I. Brändén, F. S. Mathews, F. Lederer, *J. Biol. Chem.* **266**, 3198 (1991).
27. A. T. Keatinge-Clay *et al.*, *Structure* **11**, 147 (2003).
28. R. N. Perham, *Biochemistry* **30**, 8501 (1991).
29. R. N. Perham, *Annu. Rev. Biochem.* **69**, 961 (2000).
30. K. D. Parris *et al.*, *Struct. Fold. Design* **8**, 883 (2000).
31. J. K. Stoops, S. J. Wakil, *Proc. Natl. Acad. Sci. U.S.A.* **77**, 4544 (1980).
32. K. Werkmeister, R. B. Johnston, E. Schweizer, *Eur. J. Biochem.* **116**, 303 (1981).
33. X. Huang, H. M. Holden, F. M. Raushel, *Annu. Rev. Biochem.* **70**, 149 (2001).
34. M. S. Davis, J. E. Cronan Jr., *J. Bacteriol.* **183**, 1499 (2001).
35. L. Tang, A. C. Weissborn, E. P. Kennedy, *J. Bacteriol.* **179**, 3697 (1997).
36. T. Hori, N. Nakamura, H. Okuyama, *J. Biochem.* (*Tokyo*) **101**, 949 (1987).
37. M. Sumper, D. Oesterhelt, C. Riepertinger, F. Lynen, *Eur. J. Biochem.* **10**, 377 (1969).
38. T. Maier, S. Jenni, N. Ban, *Science* **311**, 1258 (2006).
39. All data were collected at the Swiss Light Source (SLS, Paul Scherrer Institute, Villigen, Switzerland). We thank C. Schulze-Briese, A. Wagner, E. Pohl, T. Tomizaki, and S. Gutmann for their outstanding support at the SLS; our colleagues M. Steiner, B. Mikolasek, and C. Frick for their help in FAS preparation; members of the Ban laboratory for suggestions and discussions; H. Gross and W. Baumeister for their help in interpreting electron microscopic images; G. Kaim, T. Meier, U. Bauer, and A. Lehmann for assisting in cell fermentation; C. Vonrhein for a prerelease version of the program SHARP; and D. Sargent for technical assistance. *T. lanuginosus* expressed sequence tag sequence data were produced by the Fungal Genomics Project (fungalgenomics.concordia.ca). We thank A. Tsang for providing the raw sequencing data and P. Pencek for providing the cryoelectron microscopic map of the *Saccharomyces cerevisiae* FAS. S.J. was supported by the Swiss Study Foundation and thanks the instructors of the 2003 x-ray course at Cold Spring Harbor Laboratory. This work was supported by the Swiss National Science Foundation (SNSF) and the National Center of Competence in Research Structural Biology program of the SNSF. Coordinates of the rigid-body fitted homologous domains have been deposited in the Protein Data Bank with accession code 2CDH.

Grain Size–Sensitive Creep in Ice II

Tomoaki Kubo,[1]* William B. Durham,[2] Laura A. Stern,[3] Stephen H. Kirby[3]

Rheological experiments on fine-grained water ice II at low strain rates reveal a creep mechanism that dominates at conditions of low stress. Using cryogenic scanning electron microscopy, we observed that a change in stress exponent from 5 to 2.5 correlates strongly with a decrease in grain size from about 40 to 6 micrometers. The grain size–sensitive creep of ice II demonstrated here plausibly dominates plastic strain at the low-stress conditions in the interior of medium- to large-sized icy moons of the outer solar system.

High-pressure phases of water ice are major constituents of the interiors of low-density icy moons with radii of >700 km, namely Ganymede and Callisto (Jupiter); Titan, Rhea, and Iapetus (Saturn); Titania and Oberon (Uranus); and Triton (Neptune) (*1*). These moons were warmed by accretional heating and are often internally heated, either by tidal stresses of a nearby giant planet or by radioactive decay of a rocky component. The rheology of ice, as described by the relationship $\dot{\varepsilon} \propto f(\sigma)$ between a strain rate $\dot{\varepsilon}$ and differential stress σ, can control the thermal evolution and internal dynamics of icy moons (*2–6*). Typically, in crystalline solids the stress sensitivity is described by a power law, $\dot{\varepsilon} \propto \sigma^n$, where the stress exponent n is a constant. Creep experiments have been carried out at

pressure-temperature (*P-T*) conditions relevant to the interiors of icy moons to determine the flow law of several high-pressure phases (*7–12*). In those studies, differential stresses were relatively high and the grain size of samples was not controlled or examined. In all measurements to date on the high-pressure phases of ice, the stress exponent is relatively large ($n > 4$), which implies dominance of a grain size–insensitive (GSI) deformation mechanism such as dislocation creep (*13*).
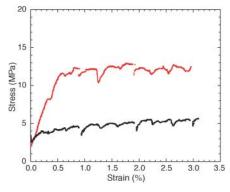
Dislocation creep may not be the dominant mechanism of deformation at the low levels of stress ($\sigma < 0.1$ MPa) expected in the convecting interiors of icy moons (*14*, *15*). According to the flow law, as stress decreases, mechanisms of lower n [particularly the contribution of grain size–sensitive (GSS) processes, such as diffusion

creep and superplasticity (*13*, *16*)] contribute proportionally more to the total strain rate than do mechanisms of higher n. For planetary applications, it is essential to identify and characterize creep mechanisms that may dominate at low stresses. We report results of creep experiments with the use of fine-grained ice II at low–strain rate conditions to 10^{-8} s^{-1}. We synthesized fine-grained ice II by rapid cycling of the transformation from ice II to ice I (II-I transformation), followed by repressurization, and observed and measured ice II grain size with the use of a cryogenic scanning electron microscope (SEM). Using these techniques, we found a low-n creep mechanism that is weaker than GSI creep in ice II and dominant at lower stresses and finer grain sizes.

Synthesis of the ice II samples and subsequent creep experiments were carried out in a cryogenic gas-medium deformation apparatus (*10*, *17*). The starting ice I (*18*) samples with a grain size of about 250 μm were transformed to ice II by pressurizing to ~300 MPa at a constant pumping rate,

[1]Department of Earth and Planetary Sciences, Faculty of Sciences, Kyushu University, Fukuoka 812-8581, Japan. [2]University of California, Lawrence Livermore National Laboratory, Livermore, CA 94550, USA. [3]U.S. Geological Survey Mail Stop 977, 345 Middlefield Road, Menlo Park, CA 94025, USA.

*To whom correspondence should be addressed. E-mail: kubotomo@geo.kyushu-u.ac.jp

Fig. 1. Stress-strain curve of ice II made by the single (red, run 516) and triple (black, run 511) I-II transformation obtained at a pressure of 200 MPa, temperature of 200 K, and constant strain rate of around 3.9×10^{-8} s^{-1} (tables S1 and S2). Breaks in the curves represent periodic unloading of the sample in order to rezero the internal force gauge. Fluctuations in the stress-strain curve are mainly due to temperature fluctuations when exchanging liquid nitrogen tanks.

ordinarily 20 to 30 MPa/min in the absence of transformation, at constant T in the range of 174 to 219 K. Large overpressures are needed at lower temperatures to initiate the I-II transformation (fig. S1). After complete I-II transformation, the pressure was vented from 300 to 30 MPa in about 5 s, which is expected on the basis of earlier experiments that produced ice I with a grain size of about 10 μm (*19, 20*). The transformation to ice II was then repeated, and in some samples a second rapid venting to ice I was performed, followed by a third transformation to ice II (table S1). We carried out deformation experiments on the samples after the first, second, or third I-II transformation (table S2). In one case (run 511), we deformed the sample after both the second and third transformations.

Six ice I samples were converted to ice II (table S1) and plastically deformed in compression at constant strain rates of 1.4×10^{-8} to 4.3×10^{-6} s^{-1} at $P = 200$ to 250 MPa and $T = 200$ to 220 K. Each run consisted of several fixed-condition steps of 1 to 3% strain, giving a total of 18 measurements of steady-state flow strength. The measured flow strength ranged from 4.0 to 22 MPa and total strains ranged from 3 to 17% (table S2). Figure 1 shows clear differences in creep behavior between ice II samples made by single and triple I-II transformations. At a constant strain rate of 3.9×10^{-8} s^{-1} (~1% strain per 3 days) and $T = 200$ K, the flow strength of the triple-transformation sample is less than half that of the single-transformation sample.

Creep results are summarized in Fig. 2. We expand the rheological relationship given above as $\dot{\varepsilon} = A\sigma^n d^{-p}\exp[-(E^* + PV^*)/RT]$, where d is grain size (diameter), and A, p, E^*, and V^* are the flow constants: preexponential factor, grain-size exponent, activation energy,
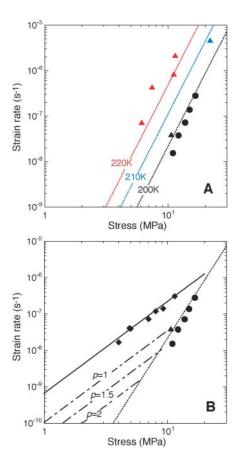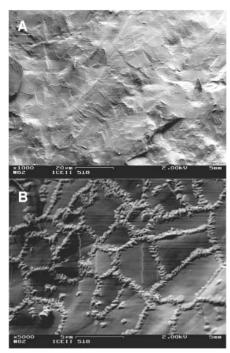

Fig. 2. Creep results for ice II with single (circle), double (triangle), and triple (diamond) I-II transformations at temperatures of 200 K (black), 210 K (blue), and 220 K (red). The grain sizes of ice II with the single and triple I-II transformations are estimated to be 38 ± 14 and 6 ± 2 μm, respectively (tables S1 and S2). Data at various pressures are adjusted to $P = 200$ MPa using an activation volume $V^* = 7$ cm³/mol (*10*). Dotted lines are the flow law with the stress exponent $n = 5.3$ previously obtained (*10*). (**A**) Creep data for ice II with single and double I-II transformations are consistent with the $n = 5.3$ rheology at 200 to 220 K. (**B**) Creep data for ice II with triple I-II transformations indicate lower flow strength and a smaller stress exponent of $n = 2.5$ (solid line) at 200 K. The dashed lines show the $n = 2.5$ rheology at a grain size of 38 μm (i.e., that of ice II after a single I-II transformation) assuming grain-size exponents of $p = 1$, 1.5, and 2. Plotted data are listed in table S2.

and activation volume, respectively. Adjusting the data at various pressures to 200 MPa using $V^* = 7$ cm³/mol (*10*), the creep data for ice II samples with single and double I-II transformations are consistent with the flow law previously obtained at $\sigma > 20$ MPa, for which $n = 5.3$ (*10*), to a lowest stress of 6.1 MPa (Fig. 2A). Ice II made by triple I-II transformation, however, shows a different rheology with a stress exponent $n = 2.5$ at $\sigma = 4.0$ to 11 MPa (Fig. 2B).
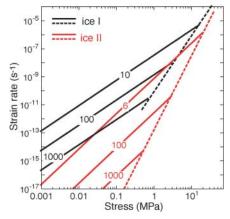
Ice II can be metastably present at 0.1 MPa and $T < 120$ K (*21*). After our creep

Fig. 3. SEM images of fractured fresh surfaces of polycrystalline ice II (*23*) showing ice II grain boundaries decorated by ice I grains. (**A**) Wide view of the sample. (**B**) Enlarged image of (A). The ice I stands in raised relief relative to the ice II due to the volumetric expansion to the lower-density phase. This ice II sample (run 518) was made by the triple I-II transformations and plastically deformed to 6% strain. After the creep experiment, the sample was partially back transformed to ice I and then quenched (tables S1 and S2) (*22*).

experiments, samples were cooled to <100 K at $P \approx 200$ MPa and then depressurized. The right-cylindrical shape of the samples (e.g., fig. S2) suggests spatial uniformity of all the processes to which the samples were subjected, including multiple transformations and several deformation steps.

The indium jackets encapsulating the samples during testing provide replicas of the outer surface of the ice samples (*11*). From SEM observations of these replicas, we estimate that the grain size of ice II samples after a single I-II transformation is 38 ± 14 μm (table S1). For the multiply transformed ice II samples, grain diameters were apparently too small for fair replication. For these samples, we decorated ice II grain boundaries by partial back transformation to ice I (*22*) and then observed the samples directly by cryogenic SEM (*23*). The networks formed by back transformation (Fig. 3) are so strongly reminiscent of grain boundaries that, in the absence of direct phase identification, we take them to be ice I grains heterogeneously nucleated on ice II grain boundaries. Furthermore, the raised relief of the ice I grains relative to ice II is in accordance with its lower density; to verify this, one sample of ice II was warmed

Fig. 4. Comparison of ice I (black) and ice II (red) rheology in both the GSI (dotted lines) and GSS (solid lines) creep regimes at 200 MPa and 200 K. Numbers are grain size (μm). Creep data for ice I were taken from previous studies (26, 27). The activation volume for GSS creep was taken as that for GSI creep in both ice I and ice II (10). GSS creep of ice II for grain sizes 100 and 1000 μm are plotted on the basis of the creep data obtained for 6 μm and assuming a grain-size exponent $p = 2$.

to above 120 K under the SEM beam. We observed the expected volumetric expansion accompanying full reversion to ice I. The size of ice II grains thus identified is 6 ± 2 μm in the sample with the triple I-II transformations and measurably smaller than the approximate 38-μm grain size achieved by single I-II transformation (table S1). The correlation between number of transformation cycles and rheology thus suggests that grain size and rheology are strongly correlated.

Another effect of repeated pressure cycling is a change in the character of the I-II transformation. Given the ~21% volume reduction of the sample (24), P can sometimes be higher before the transformation than afterwards. We detected the I-II transformation during pressurization by deviations from the normal P-versus-time trend at a steady rate of pumping. These deviations become increasingly sharp with repeated phase transformations (fig. S3 and table S1). If the sharpness is related inversely to grain size as the SEM observations suggest, then the grain size after the second I-II transformation, which was not observed by SEM, might be expected to be between 38 and 6 μm.

We demonstrate a change from a GSI to a weaker GSS rheology at low stresses and finer grain sizes in ice II. As Fig. 2B shows, at 200 MPa and 200 K, the fine-grained ice II of $d \approx$ 6 μm is much weaker than ice II of $d \approx$ 40 μm. Furthermore, the finer-grained material has a distinctly lower stress exponent than does the coarse-grained material: $n = 2.5$ versus $n = 5.3$. We estimate roughly a grain-size exponent $p >$ 1.5 on the basis of the dashed lines in Fig. 2B; if p were <1.5, the lowest circle in Fig. 2B (ice II of $d = 38$ μm, the single I-II transition, at the

lowest strain rate of 1.6×10^{-8} s^{-1}) would reflect the transition to GSS creep and would be shifted to lower stresses.

Ice II with grain size of about 15 μm shows that grain size induced weakening (19), which is consistent with our results. GSS creep has been reported in ice I at ambient conditions (25, 26). The flow law of GSS creep found in various materials including ice I is generally characterized by a smaller stress exponent $n \approx$ 2 instead of $n \approx$ 5 for dislocation creep, and a grain-size exponent of $p \approx$ 2 (13, 16). GSS creep in ice II with stress exponent $n = 2.5$ is consistent with these previous studies.

Figure 4 is a comparison of GSI and GSS rheologies for both ice I and ice II at 200 MPa and 200 K. For a given grain size, ice II is stronger than ice I for both creep mechanisms. For $d \approx$ 10 μm, a transition from GSI creep to GSS creep occurs at $\sigma \approx$ 10 MPa in both ice I and ice II. Assuming a typical grain-size exponent of $p = 2$ for GSS creep in ice II, extrapolation of the flow law to more planetary-relevant grain sizes of $d = 1$ and 10 mm suggests that GSS creep becomes dominant at $\sigma < 0.5$ and 0.1 MPa, respectively; for $p = 1.5$, the transition to GSS creep in ice II occurs at $\sigma = 1$ and 0.5 MPa, respectively.

The stress levels in the density-driven, convecting interiors of medium- and large-size icy moons have been estimated to be on the order of 0.01 MPa (14) and 0.1 MPa (15), respectively. Therefore, it is likely that both ice I and ice II plastically deform by the GSS creep mechanisms in the interior of icy moons when the grain size is less than 10 mm. In Fig. 4, for example, at a stress of 0.1 MPa and grain size of 1 mm, the viscosities ($\sigma/3\dot{\varepsilon}$) for GSI creep in ice II, GSS creep in ice II, and GSS creep in ice I are 5.2×10^{22}, 4.7×10^{20}, and 4.4×10^{16} Pa·s, respectively, at a pressure of 200 MPa and temperature of 200 K. The viscosity contrast between ices I and II at the I-II transition depth will therefore be about four orders of magnitude (ice II is the stronger of the two) if the ice II is deforming in GSS creep and six orders of magnitude if GSS creep is suppressed. The difference in flow patterns and heat transfer in the interiors will be substantial. Thus, although further quantitative investigations of the grain-size and temperature dependence are needed, the GSS creep of ice II demonstrated in this study is a possible candidate for a flow mechanism that controls the thermal evolution and internal dynamics of medium- and large-size satellites of the outer planets.

References and Notes
1. D. A. Rothery, *Satellites of the Outer Planets* (Oxford Univ. Press, New York, 1999).
2. G. L. Consolmagno, J. S. Lewis, *Icarus* **34**, 280 (1978).
3. R. T. Reynolds, P. M. Cassen, *Geophys. Res. Lett.* **6**, 121 (1979).
4. J. P. Poirier, *Nature* **299**, 683 (1982).
5. G. Schubert, T. Spohn, R. T. Reynolds, in *Satellites* (Univ. Arizona Press, Tucson, AZ, 1986), pp. 242–292.
6. W. B. McKinnon, in *Solar System Ices* (Kluwer, Dordrecht, Netherlands, 1998), pp. 525–550.
7. J. P. Poirier, C. Sotin, J. Peyronneau, *Nature* **292**, 225 (1981).
8. C. Sotin, P. Gillet, J. P. Poirier, in *Ices in the Solar System*, J. Klinger *et al.*, Eds. (D. Reidel, Hingham, MA, 1985), pp. 109–118.
9. C. Sotin, J. P. Poirier, *J. Phys.* **48**, 233 (1987).
10. W. B. Durham, S. H. Kirby, H. C. Heard, L. A. Stern, C. O. Boro, *J. Geophys. Res.* **93**, 10191 (1988).
11. W. B. Durham, L. A. Stern, S. H. Kirby, *J. Geophys. Res.* **101**, 2989 (1996).
12. K. Echelmeyer, B. Kamb, *Geophys. Res. Lett.* **13**, 693 (1986).
13. J. P. Poirier, *Creep of Crystals* (Cambridge Univ. Press, Cambridge, 1985).
14. K. Ellsworth, G. Schubert, *Icarus* **54**, 490 (1983).
15. G. Schubert, D. J. Stevenson, K. Ellsworth, *Icarus* **47**, 46 (1981).
16. J. W. Edington, K. N. Melton, C. P. Cutler, *Prog. Mater. Sci.* **21**, 61 (1976).
17. H. C. Heard *et al.*, in *Geophys. Monogr. Am. Geophys. Union 56*, A. G. Duba *et al.*, Eds. (American Geophysical Union, Washington, DC, 1990), pp. 225–228.
18. Starting materials are molded synthetic ice I aggregates, 63 mm long and 25 mm in diameter with a grain size of about 250 μm (19). The starting sample has a uniform texture with virtually no porosity and a random grain orientation.
19. L. A. Stern, W. B. Durham, S. H. Kirby, *J. Geophys. Res.* **102**, 5313 (1997).
20. W. B. Durham, L. A. Stern, S. H. Kirby, *J. Geophys. Res.* **106**, 11031 (2001).
21. J. E. Bertie, L. D. Calvert, E. Whalley, *J. Chem. Phys.* **38**, 840 (1963).
22. After the creep experiments in the stability field of ice II, the pressure was slowly decreased to the ice I stability field at the rate of about 7 MPa/min at constant temperature of 200 K. When the back II-I transition started at about 140 MPa, which was identified from the slight slowing of the rate of pressure decrease, the pressure was increased back to that at the I-II phase boundary. The sample length, which can be measured by the piston contact to the sample (11), showed slight lengthening due to the partial back transformation. The sample was then cooled along the I-II phase boundary to <100 K, depressurized, removed from the vessel, and stored at 77 K.
23. SEM observations were conducted on the uncoated sample with a cryogenic stage at temperatures of less than 100 K and low accelerating voltage of 2 kV with the use of a LEO 982 field emission SEM. Before imaging, the sample was fractured with a cold blade at 100 K under vacuum to produce fresh surfaces that were not contaminated by surface condensation.
24. N. H. Fletcher, in *The Chemical Physics of Ice* (Cambridge Univ. Press, Cambridge, 1970), p. 57.
25. D. L. Goldsby, D. L. Kohlstedt, *Scr. Mater.* **37**, 1399 (1997).
26. D. L. Goldsby, D. L. Kohlstedt, *J. Geophys. Res.* **106**, 11017 (2001).
27. W. B. Durham, S. H. Kirby, L. A. Stern, *J. Geophys. Res.* **102**, 16293 (1997).
28. We thank R. Oscarson and J. Pinkston of the U.S. Geological Survey (USGS) for their technical assistance and I. M. Chou and D. Moore (USGS) for helpful reviews of the manuscript. This work was supported by the Japan Society for the Promotion of Science postdoctoral fellowships for research abroad and the grant for basic science research projects of The Sumitomo Foundation (to T.K.) and by NASA under order W-19,868. Work was performed under the auspices of the U.S. Department of Energy by the Lawrence Livermore National Laboratory under contract W-7405-ENG-48.